

# Observations of the Corona Borealis supercluster with the superextended Very Small Array: further constraints on the nature of the non-Gaussian CMB cold spot

Ricardo Génova-Santos,<sup>1,2\*</sup> José Alberto Rubiño-Martin,<sup>2</sup> Rafael Rebolo,<sup>2,4</sup> Richard A. Battye,<sup>3</sup> Francisco Blanco,<sup>3</sup> Rod D. Davies,<sup>3</sup> Richard J. Davis,<sup>3</sup> Thomas Franzen,<sup>1</sup> Keith Grainge,<sup>1</sup> Michael P. Hobson,<sup>1</sup> Anthony Lasenby,<sup>1</sup> Carmen P. Padilla-Torres,<sup>2</sup> Guy G. Pooley,<sup>1</sup> Richard D.E. Saunders,<sup>1</sup> Anna Scaife,<sup>1</sup> Paul F. Scott,<sup>1</sup> David Titterington,<sup>1</sup> Marco Tucci<sup>2</sup> and Robert A. Watson<sup>3</sup>

<sup>1</sup> *Astrophysics Group, Cavendish Laboratory, University of Cambridge CB3 0HE, UK*

<sup>2</sup> *Instituto de Astrofísica de Canarias, 38200 La Laguna, Tenerife, Canary Islands, Spain*

<sup>3</sup> *Jodrell Bank Centre for Astrophysics, University of Manchester, Manchester M13 9PL, UK*

<sup>4</sup> *Consejo Superior de Investigaciones Científicas, Spain*

Accepted Received In original form

## ABSTRACT

We present interferometric imaging at 33 GHz, with the new superextended configuration of the Very Small Array (VSA), of a very deep decrement in the cosmic microwave background (CMB) temperature. This decrement is located in the direction of the Corona Borealis supercluster, at a position with no known galaxy clusters, and was discovered by a previous VSA survey (Génova-Santos et al.). A total area of 3 deg<sup>2</sup> has now been imaged, with an angular resolution of 7 arcmin and a flux sensitivity of 5 mJy beam<sup>-1</sup>.

These observations confirm the presence of this strong and resolved negative spot at  $-41 \pm 5$  mJy beam<sup>-1</sup> ( $-258 \pm 29$   $\mu$ K), with a signal to noise level of 8. This structure is also present in the WMAP 5-year data. The temperature of the W-band (94 GHz) data at the position of the decrement agrees within  $1.2\sigma_n$  with that observed by the VSA at 33 GHz, and within  $0.2\sigma_n$  with the Sunyaev-Zel'dovich (SZ) spectrum.

Our analyses show that it is a non-Gaussian feature in the CMB at a level of  $4.8\sigma$ . The probability of finding such a deviation or larger in CMB Gaussian simulations is only 0.19 per cent. Therefore, an explanation other than primordial CMB is required. We have considered the possibility of an SZ effect generated in a diffuse, extended warm/hot gas distribution. This hypothesis is especially relevant, as the presence of such structures, if confirmed, could provide the location for a significant fraction of the missing baryons in the Local Universe.

**Key words:** techniques: interferometric – galaxies: clusters: general – cosmic microwave background – cosmology: observations.

## 1 INTRODUCTION

The baryon density at  $z = 0$ , derived from the total budget over the well-observed components (Fukugita et al. 1998), is a factor  $\approx 2$  lower than that at high redshift, inferred through independent methods, namely big bang nucleosynthesis

(Burles et al. 2001), the Ly $\alpha$  forest (Rauch et al. 1997) and the cosmic microwave background (CMB) primary anisotropies (e.g. Rebolo et al. 2004; Dunkley et al. 2008). According to the results of hydrodynamical simulations (Cen & Ostriker 1999; Davé et al. 2001; Cen & Ostriker 2006) a substantial fraction of these missing baryons could be located in the so-called ‘warm/hot intergalactic medium’ (WHIM). This is a very diffuse gas phase, arranged in sheet-

\* E-mail: rgs@mrao.cam.ac.uk

like or filamentary structures, with temperatures  $10^5 \leq T \leq 10^7$  K, typical baryon overdensities in the range  $\delta\rho_B/\langle\rho_B\rangle \sim 10 - 30$ , and length scales of the order of 10 Mpc. Its intermediate temperature and low density, in conjunction with the presence of many Galactic foregrounds and different extragalactic contaminants, make the detection of the WHIM rather challenging. Several attempts (some of which have produced tentative detections) have been carried out, either by looking for its possible soft X-ray emission (Soltan et al. 2002; Finoguenov et al. 2003; Zappacosta et al. 2005) or by identifying UV (Nicastro et al. 2002, 2005) or soft X-ray (Barcons et al. 2005) absorption lines in the spectra of more distant sources.

The thermal Sunyaev–Zel’dovich (SZ) effect (Sunyaev & Zeldovich 1972) has been proposed, and in fact used, as an alternative tool to search for this hidden matter. This is a secondary anisotropy of the CMB due to the inverse Compton scattering of its photons by high-energy electrons such as those located in the extended atmospheres of hot gas ( $k_B T_e \sim 10$  keV) of the richest clusters of galaxies. The SZ signal is proportional to the line-of-sight integral of the electron density multiplied by the electron temperature. This effect is well known and many detections have been achieved over the last decade in nearby clusters (see e.g. Birkinshaw 1999; Carlstrom, Holder & Reese 2002). Structures like superclusters of galaxies, where the WHIM is likely to be located, could also build up a significant SZ effect (Birkinshaw 1999). Their lower baryon overdensities are compensated for by the long path-lengths of the CMB photons across them. Indeed, Hernández-Monteagudo et al. (2006) concluded from the results of a numerical simulation that  $\approx 15\%$  of the SZ signal on the sky would be generated in this kind of structure. Many studies have been carried out to identify statistical detections of diffuse intra-supercluster (ISC) gas through its likely SZ effect, making use of the *COBE*-DMR (Banday et al. 1996) or WMAP (Fosalba, Gaztañaga, & Castander 2003; Hernández-Monteagudo & Rubiño-Martín 2004; Myers et al. 2004; Hernández-Monteagudo, Génova-Santos & 2004) datasets. However, there have been no clear detections to date.

In this context, we selected the Corona Borealis supercluster (CrB-SC) for observations at 33 GHz with the VSA extended configuration (Génova-Santos et al. 2005, hereafter GS05). These were the first targeted observations searching for extended SZ in the direction of this kind of structure. We found a clear negative feature, which we called “decrement H” with a flux density  $-103 \pm 10$  mJy beam $^{-1}$  ( $-230 \pm 23$   $\mu$ K) and coordinates RA =  $15^h 22^m 11.47^s$ , Dec. =  $+28^\circ 54' 06.2''$  (J2000), in a region with no known clusters. Our analyses ruled out, at a level of 99.6%, the explanation of this decrement based only on a primary CMB anisotropy. This led us to consider an extended SZ effect generated by a filamentary structure consisting of warm/hot gas. The possibility of an SZ effect from an unknown background cluster was also considered, but this is rather unlikely due to the large angular size of the decrement, which could only be generated by a nearby cluster. The absence of significant X-ray emission in this region in the *ROSAT* XRT/PSPC All-Sky Survey map set constraints on the physical characteristics of the hypothetical filamentary structure, making it very unlikely that it could generate such a big SZ decrement on its

own. Therefore, the most plausible hypothesis is a combination of a negative primary anisotropy and an extended SZ effect.

This work was followed by an observational campaign in this region with the MITO telescope at 143, 214, 272 and 353 GHz (Battistelli et al. 2006). The results of the analyses of the three lowest frequency channels, in conjunction with the VSA map at 33 GHz, support the hypothesis of a combination of a primary CMB anisotropy with an extended SZ effect, the relative contribution of the latter component being  $0.25^{+0.21}_{-0.18}$ . The decrement seems to be unresolved by the MITO beam (FWHM  $\approx 16'$ ), and is detected in the three lowest frequency channels.

In the present work we have carried out observations in the region of this decrement with the newly superextended configuration of the VSA, which has a factor  $\approx 2$  finer angular resolution than the extended configuration used in the previous observations.

In Section 2 we present a description of the VSA interferometer, emphasizing the differences between the superextended and the previous configurations. In Section 3 we describe the observations and the data reduction procedure and in Section 4 we present the final maps. Section 5 includes the discussion about the possible origins of the decrement, and conclusions are presented in Section 6.

## 2 THE SUPEREXTENDED VSA

The VSA is a 14-element heterodyne interferometer, tunable between 26 and 36 GHz with a bandwidth of 1.5 GHz, sited at the Teide Observatory in Tenerife, at an altitude of 2400 m. Currently it observes at a central frequency of 33 GHz, with a system temperature of approximately 25 K. A detailed description of the instrument can be found in Watson et al. (2003). Its main target has been the observations of the primary anisotropies of the CMB, aimed at estimating the CMB power spectrum (Scott et al. 2003; Grainge et al. 2003; Dickinson et al. 2004), although it has also been successfully used to observe the SZ effect in nearby clusters of galaxies (Lancaster et al. 2005).

The VSA has observed with three different sets of antennas. The compact array, used from October 2000 to September 2001, was sensitive in the multipole range  $\ell \sim 150 - 900$  and had antenna apertures providing a primary beam of  $4.6$  FWHM. In October 2001 this was replaced with the extended array, sensitive in the multipole range  $\ell \sim 300 - 1500$  and with a  $2.1$  FWHM primary beam. In 2005 the antenna centres were repositioned and the mirrors replaced to provide a  $1.2$  FWHM primary beam. This superextended array covers the multipole range  $\ell \sim 350 - 2450$ , and produces a synthesized beam of  $\approx 7$  arcmin FWHM. Currently it is chiefly dedicated to the observations of primordial fields with the objective of investigating the power excess discovered by CBI at  $\ell = 2000 - 4000$  (Mason et al. 2003).

Situated next to the main array are the two 3.7-m source-subtractor (SS) antennas for simultaneous monitoring of radio sources, providing fluxes at 33 GHz on these sources, which are then subtracted from the main array data. This is a two-element interferometer giving a resolution of 4 arcmin in a 9 arcmin field.

**Table 1.** Summary of the observations with the VSA. We list the central coordinate of the 6 pointings, the total observation time, the integration time and the achieved thermal noise (computed from the map far outside the primary beam).

Pointing	RA (J2000)	Dec. (J2000)	T <sub>obs</sub> (hr)	T <sub>int</sub> (hr)	Thermal noise (mJy beam <sup>-1</sup> )
CrB-H	15 23 00.00	29 13 30.0	50	33	6.8
CrB-H-spot	15 22 11.47	28 54 06.2	145	75	4.2
CrB-H-spotN	15 22 11.47	29 24 06.2	25	8	18.3
CrB-H-spotS	15 22 11.47	28 24 06.2	25	11	15.0
CrB-H-spotE	15 23 56.47	28 54 06.2	15	6	17.9
CrB-H-spotW	15 20 26.47	28 54 06.2	15	6	23.2

### 3 OBSERVATIONS AND DATA REDUCTION

#### 3.1 Observations

The observations were carried out mainly during the periods: i) October and November 2005; and ii) May and June 2006. We defined 6 pointings, which are listed in Table 1 along with their coordinates. The field CrB-H has the same coordinates as the corresponding pointing in the previous observations with the extended configuration (GS05). It was in this field that the decrement H was detected at the highest level of significance. The pointing CrB-H-spot is centred on the position where decrement H was found in those observations. With the aim of producing a final larger mosaic, we defined four additional pointings with coordinates shifted in right ascension and declination. In Table 1 we also quote both total observation and integration times (the latter indicating the amount of data retained after flagging), and the thermal noise achieved in each field. Most of the observation time was spent on the central fields CrB-H and CrB-H-spot. The fractional amount of useful data in the fields CrB-H and CrB-H-spot exceeds 50%, but in the four additional fields it is considerably lower. This is due to the fact that the latter four fields were observed at higher hour angles, where the quality of the data is worse, and therefore a larger amount of data had to be discarded. The noises are consistent with the total integration time in each field.

#### 3.2 Calibration and data reduction

The absolute flux calibration of VSA data is determined from observations of Jupiter, whose brightness temperature is taken from the WMAP 5-year data:  $T_{\text{Jup}} = 146.6 \pm 0.7$  K (Hill et al. 2008). This flux scale is transferred to other calibration sources: Tau A and Cas A. A detailed description of the VSA calibration process is presented in Watson et al. (2003). The specifications for the superextended configuration (such as the correction for the fact that Tau A and Cas A are partially resolved in the longest baselines) are essentially the same as those adopted for the extended configuration, and are explained in Dickinson et al. (2004). As a further improvement to these processes for the present configuration, a secondary phase calibration provided by short calibration observations (on Cas A in the observations presented in this work), interleaved with the main field observations, was introduced.

The data reduction pipeline followed essentially the one described in Dickinson et al. (2004). However, in the su-

perextended configuration data some further systematics have been identified. Some of the daily maps showed stripes. This is due to the low quality of the data on the shortest baselines at extreme hour angles (around  $\pm 2$ h), detected only when stacking the whole dataset in hour angle, but not on the individual days. By flagging relevant hour angle intervals in these baselines the stripes are removed.

#### 3.3 Source subtraction

The source subtraction was carried out similarly to GS05. This involves extrapolation to 33 GHz of the fluxes of all the sources found in the NVSS–1.4 GHz (Condon et al. 1998) and GB6–4.85 GHz (Gregory et al. 1996) catalogues. In the present observations, due to the narrower primary and synthesized beams, we focus on sources closer than  $1.2^\circ$  from the pointing centres and brighter than 18 mJy at 33 GHz. We found that all the identified sources had measured fluxes above this level, as quoted in Table 2. These values were subtracted from the data, and were obtained, using the same estimator as in GS05, from the SS observations performed simultaneously with the extended configuration observational campaign (during the periods May 2003–February 2004 and August 2004–November 2004).

This strategy has two main drawbacks. First, as the detection limit of the GB6 catalogue is 18 mJy, we are missing all the sources with inverted spectra between 4.85 GHz and 33 GHz, which may be of the order of 20% of all the sources (Waldram et al. 2003). This implies that we could be missing around one radio source due to this. Second, we are subtracting fluxes that have been derived from SS observations carried out two years before the observations of the main array. Therefore, variability can be important here, and to assess it we have applied a  $\chi^2$ -test to each source. The values of  $\chi^2$  quoted in Table 2 have been calculated as

$$\chi^2 = \sum_{i=1}^{N_{\text{obs}}} \left( \frac{S_i - S_{\text{meas}}}{\Delta S_i} \right)^2, \quad (1)$$

where  $N_{\text{obs}}$  is the total number of observations for each source,  $S_i$  and  $\Delta S_i$  are the value and the error of each individual measurement and  $S_{\text{meas}}$  is the final averaged value. This tests the hypothesis that the flux-density time-series could be modelled as a constant. Following Bolton et al. (2006), we considered as variable the sources for which the probability of obtaining an equal or higher value in a  $\chi^2$  distribution with  $N_{\text{obs}} - 1$  degrees of freedom is less than 1 per cent. According to this only the source 1522+2808 is

**Table 2.** List of all the radio sources with measured fluxes at 33 GHz above 18 mJy. We quote the extrapolated flux at 33 GHz, and the estimated flux at 33 GHz using the SS observations, which have been used to subtract the sources from the data. In the last three columns we list the number of individual observations for each source, the fractional variation (per cent) of the fluxes on these individual observations and the result of the  $\chi^2$  test.

Name	RA (J2000)	Dec. (J2000)	$S_{\text{ext}}$ (mJy)	$S_{\text{meas}}$ (mJy)	$N_{\text{obs}}$	$\Delta S/S$ (%)	$\chi^2$
1516+2918	15 16 40.9	29 18 25.0	37	$37 \pm 7$	16	50.4	6.0
1519+2746	15 19 51.0	27 46 23.0	33	$34 \pm 16$	4	82.1	3.1
1521+2830	15 21 04.8	28 30 29.0	87	$34 \pm 4$	32	62.5	36.3
1522+2808	15 22 48.9	28 08 51.0	135	$97 \pm 3$	118	40.0	172.3
1523+2836	15 23 27.9	28 36 51.0	62	$32 \pm 3$	61	78.9	45.8
1524+2900	15 24 04.2	29 00 22.0	57	$32 \pm 3$	76	65.2	45.7
1527+2855	15 27 44.7	28 55 24.0	38	$35 \pm 7$	17	68.8	12.1

classified as variable. Its fractional variation, calculated as

$$\frac{\Delta S}{S_{\text{meas}}} = \frac{1}{S_{\text{meas}}} \sqrt{\frac{\sum S_i^2 / (\Delta S_i)^2}{\sum 1 / (\Delta S_i)^2} - \left( \frac{\sum S_i / (\Delta S_i)^2}{\sum 1 / (\Delta S_i)^2} \right)^2}, \quad (2)$$

is 40%. However, this source lies at a distance of  $0.77^\circ$  from the CrB-H-spot pointing (this is the most important pointing in our analysis, as will become clear), where the primary beam attenuation is a factor 0.32, so the consequences of its variability are ameliorated. To check this we have subtracted this radio source from the observed map using the two extreme fluxes given by the estimated flux plus and minus its variability, and found that the flux difference in the centre of the map is only 1.3%.

We have estimated the confusion noise due to unresolved sources below our source subtraction threshold of 18 mJy by using the formalism of Scheuer (1957) and the best-fitting power-law model obtained from the source count of the whole sample of sources in GS05. We found  $\sigma_{\text{sour}} = 3.8 \text{ mJy beam}^{-1}$  – this value is lower than the thermal noise in any of the fields.

#### 4 VSA MAPS

Daily observations, after being calibrated and reduced, are held as visibility files. These files are loaded individually into AIPS, where the final stack for each field is made. Source subtraction is then applied in the aperture plane, and maps are produced for each pointing using standard AIPS tasks. Since we are interested in extended structures, we typically use natural weighting. The deconvolution of the synthesized beam is carried out using standard AIPS tasks down to a depth about the noise level. CLEAN boxes are placed around the position of decrement H, and around the radio sources in the non-source-subtracted maps.

The CLEANed maps built up from pointing CrB-H-spot, before and after source subtraction, are shown in the top panels of Fig. 1. Decrement H is clearly detected (signal-to-noise level of 8), with a peak negative flux density  $-41 \pm 5 \text{ mJy beam}^{-1}$  (with a  $7.7 \times 6.5 \text{ arcmin}^2$  beam; brightness temperature of  $-258 \pm 29 \mu\text{K}$ ) at RA =  $15^{\text{h}}22^{\text{m}}11.47^{\text{s}}$ , Dec. =

$+29^\circ00'06.2''$  (J2000)<sup>1</sup>, and with angular size of about  $30 \times 20 \text{ arcmin}^2$ .

In order to enhance the large angular scales, we have applied a Gaussian taper function of width  $\sigma = 150\lambda$  to the visibilities. In the resulting map, which is shown in the bottom-left corner of Fig. 1, the detection of decrement H is even more remarkable, with a minimum flux density of  $-101 \pm 18 \text{ mJy beam}^{-1}$  (with a  $15.3 \times 10.5 \text{ arcmin}^2$  beam; brightness temperature of  $-197 \pm 35 \mu\text{K}$ ). At this resolution, around the peak decrement there are  $\approx 2$  contiguous resolution elements each with negative flux exceeding  $5\sigma_n$  (being  $\sigma_n$  the thermal noise of the map), corresponding to an integrated decrement flux of  $-180 \pm 19 \text{ mJy}$ ; another measure of the overall decrement is that there are  $\approx 4$  contiguous resolution elements with negative flux exceeding  $3\sigma_n$ , corresponding to an integrated decrement of  $-277 \pm 26 \text{ mJy}$ .

We have also combined the individual overlapping maps of the six independent pointings to produce the final source-subtracted mosaic shown in the bottom-right corner of Fig. 1. In order to avoid the loss of signal-to-noise ratio, and given that the synthesized beams of the six pointings have similar shapes and orientations, here we have applied the CLEANING to the whole mosaic instead of to the individual pointings. To this end, we used the synthesized beam of the pointing CrB-H-spot and placed a CLEAN box around the decrement.

In all these maps the decrement is resolved by the VSA synthesized beam. This can be clearly seen in Fig. 2, where we plot the angular profiles of both the decrement and the restoring beam. We have plotted both the radial-averaged profiles (left) and the profiles along a line oriented in northeast-southwest direction (right), where the decrement shows the greatest elongation. It can be seen that there is some substructure, with a secondary minimum towards the northeast, at a position RA =  $15^{\text{h}}22^{\text{m}}36.64^{\text{s}}$ , Dec. =  $+29^\circ04'06.0''$  (J2000).

These results represent a successful confirmation, from a completely independent dataset, of the previous detection with the VSA extended configuration. In Fig. 3 we show a

<sup>1</sup> This minimum flux value and coordinates (and also other fluxes and coordinates presented hereafter) have been obtained from the dirty map. This is reliable as the CLEANING procedure only affects the regions of the map surrounding the decrement, where the CLEAN box has been positioned. Therefore, the minimum flux of the decrement may remain the same after the CLEANING.

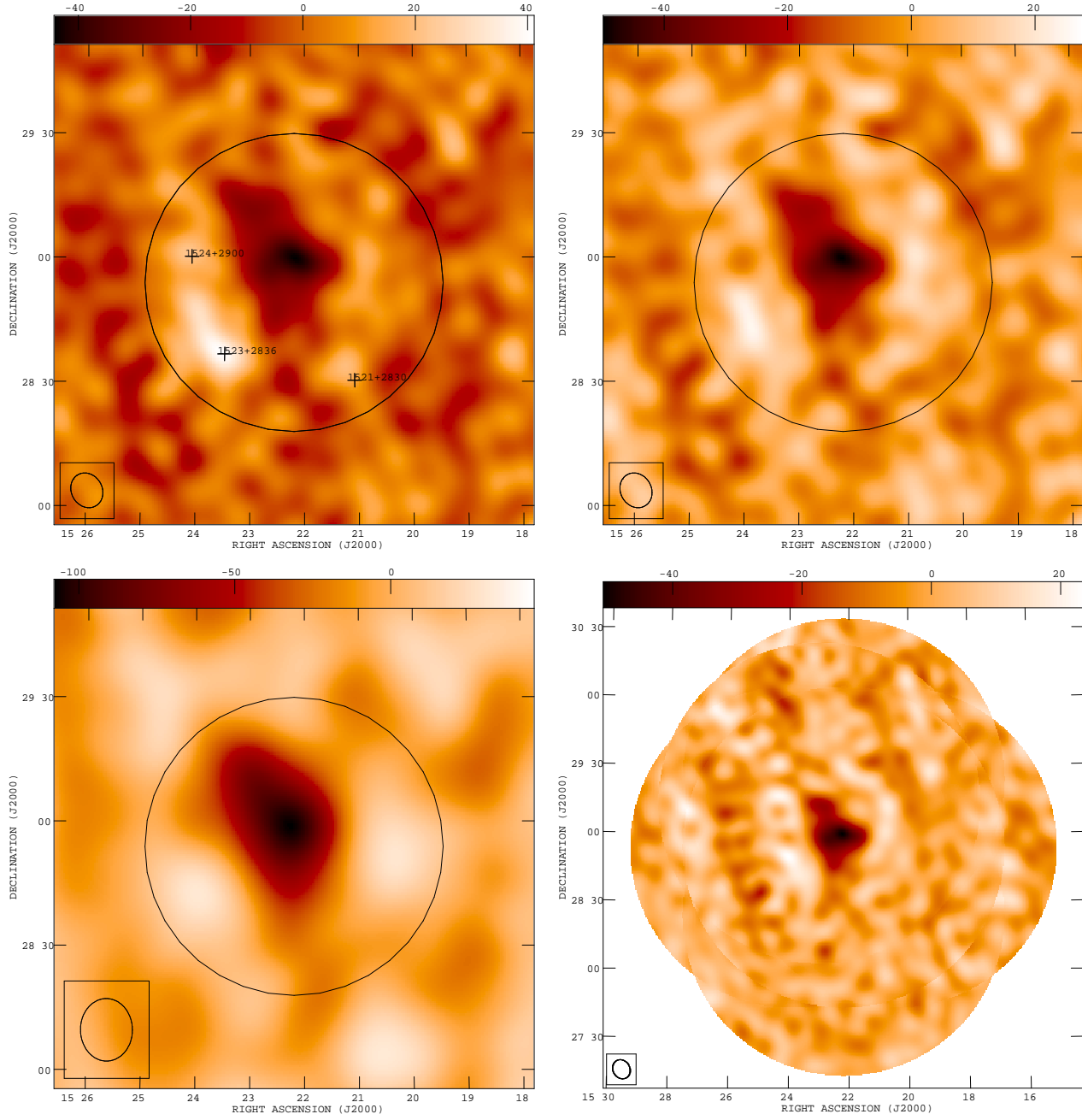


**Figure 1.** CLEANED maps of the decrement  $H$  in the CrB-SC obtained with the VSA superextended configuration. Top: maps of pointing CrB-H-spot before (left) and after (right) source subtraction. In the non-source-subtracted map the crosses show the positions of the monitored radio sources inside the primary beam FWHM. Bottom left: source-subtracted map of pointing CrB-H-spot, after applying a Gaussian taper of  $\sigma = 150\lambda$  in the  $uv$  plane. The circle indicates the primary beam FWHM ( $1.2^\circ$ ) of the CrB-Hspot pointing. Bottom right: CLEANED VSA mosaic built up from the six pointings listed in Table 1. The noise level is practically uniform across the mosaic at a level  $\approx 5$  mJy beam $^{-1}$ . The units of the colour-scale shown in the top bar are mJy beam $^{-1}$ . The synthesized beam FWHM is shown in the bottom-left corner of each map.

comparison of the maps in the region of the decrement resulting from both observational campaigns. Despite that in both cases different angular scales are sampled in the aperture plane of our observations, the two maps are consistent, and the shape of the structure is similar in them. In order to assess the compatibility of the measurements of the minimum brightness temperature in both observations, we have applied a Gaussian taper function of width  $\sigma = 170\lambda$  to the

superextended visibilities. This taper function produces a synthesized beam comparable to that of the extended observations. The minimum flux decrement in this map is  $-90 \pm 14$  mJy beam $^{-1}$  (with a  $13.9 \times 10.3$  arcmin $^2$  beam; brightness temperature of  $-196 \pm 30$   $\mu$ K), whereas the minimum flux decrement in the extended map is  $-117 \pm 15$  mJy beam $^{-1}$  (with a  $14.0 \times 10.2$  arcmin $^2$  beam; brightness temperature

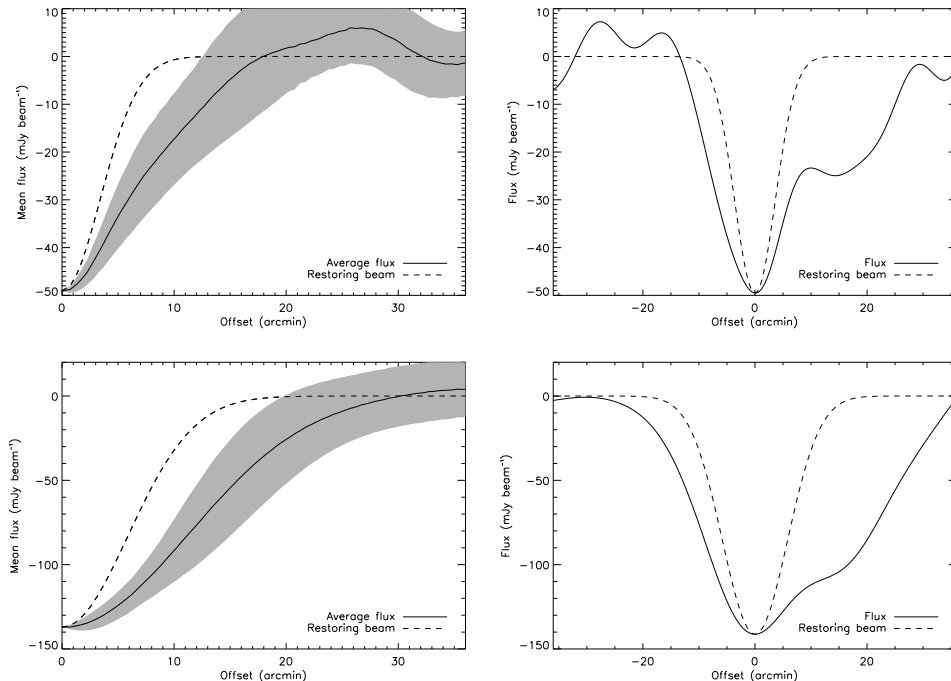


**Figure 2.** Angular profiles of the decrement H in the CLEANED and source-subtracted maps of pointing CrB-H-spot (solid line) and of the restoring beam (dashed line). We represent cases when no tapering is used (top) and when a Gaussian taper of  $\sigma = 150\lambda$  is applied to the data (bottom). Left plots show the average flux in rings of increasing radius from the position of the minimum flux of the decrement, whereas right plots represent the flux along a NE-SW line. In the left plots the shaded regions show the  $1\sigma$  error in each ring.

of  $-255 \pm 33 \mu\text{K}$ <sup>2</sup>. Therefore, both measurements agree to within  $1.3\sigma$ .

## 5 ORIGIN OF THE DECREMENT

In GS05 we presented a detailed discussion about the possible origin of decrement H, considering three different scenarios: a primary CMB anisotropy, an unknown cluster of galaxies and a concentration of WHIM gas. Our statistical analyses yielded a probability of 0.38% for a primary anisotropy, while only  $\approx 0.3$  clusters rich enough to produce such a deep decrement are expected in the entire surveyed region ( $\approx 24 \text{ deg}^2$ ). This cluster hypothesis is further disfavoured by the fact that, due to the absence of any excess of X-ray emission in the *ROSAT* data, a distant cluster would be needed, and this is in conflict with the large angular extension of the decrement. Furthermore, we have recently carried out an optical survey with the ING telescope that has not shown any evidence of a cluster in the region of the CrB-SC (Padilla-Torres et al. 2008, in prep.). A high concentration of infrared galaxies at a redshift  $z \approx 0.11$  was found, but with a physical distribution unlike that of clusters of galaxies. The absence of X-ray emission also set constraints

on the physical characteristics that a WHIM structure may have. This indeed rules out the possibility of a diffuse structure, with a depth of the order of the maximum separation along the line of sight between clusters in the core of CrB-SC ( $\approx 40 \text{ Mpc}$ ), and with electron temperature typical of WHIM. Therefore, we concluded that the most plausible hypothesis is a combination of primordial CMB fluctuations with an SZ effect from a large-filamentary structure oriented in a direction close to the line of sight. We now revisit these analyses after bringing in the new superextended configuration data.

In order to assess the possible contribution from the primordial CMB to this deep decrement, we repeated the Monte Carlo analysis described in GS05, but now using as template in the aperture plane the visibility points sampled by the CrB-H-spot pointing. We carried out 15000 simulations, adding to each three components: primordial CMB, thermal noise and residual radio sources below the subtraction threshold of 18 mJy. For the first of these components, the input power spectrum was generated up to  $\ell = 3000$  with CAMB (Lewis et al. 2000), from a cosmological model defined by the following parameters:  $\Omega_B = 0.044$ ,  $\Omega_M = 0.25$ ,  $\Omega_\Lambda = 0.75$ ,  $h = 0.73$ ,  $\tau = 0.14$ ,  $10^{10} A_S = 23$ ,  $n_S = 0.97$ , as derived from the most recent VSA results (Rebolo et al. 2004), plus  $T_{\text{CMB}} = 2.725 \text{ K}$  (Mather et al. 1999) and  $\Omega_\nu = 0$ . For the thermal noise we performed realizations using the actual noise values in the visibility template. Finally, the residual radio sources were simulated, in the aperture plane and within  $1.2^\circ$  of the field centre, following the source count derived from the flux values obtained

<sup>2</sup> Note that these fluxes and temperatures have been corrected by the primary beam response, which is necessary here as the pixel with the minimum flux lies at different distances from the pointing centres in the extended and superextended observations. This is why the extended flux and temperature values are different from those presented in GS05, where no primary beam correction was applied and the CLEAN map was used.

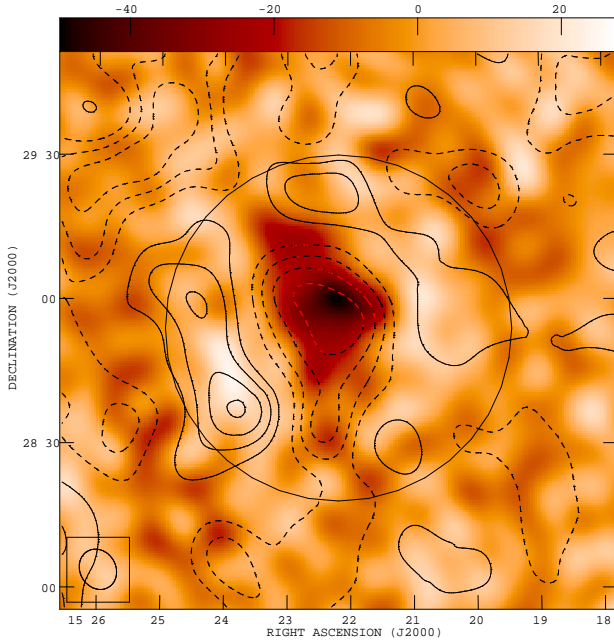


**Figure 3.** Comparison of the source-subtracted and CLEANED maps of decrement H obtained with the VSA extended configuration (contours) and with the VSA superextended configuration (colour scale). The units of the superextended map, shown in the top bar, are  $\text{mJy beam}^{-1}$ . The difference between contours in the extended map is  $18 \text{ mJy beam}^{-1}$  ( $1.5\sigma_n$ ). The circle around the centre and the ellipse in the bottom-left corner indicate respectively the FWHM of the primary and synthesized beams of the superextended map.

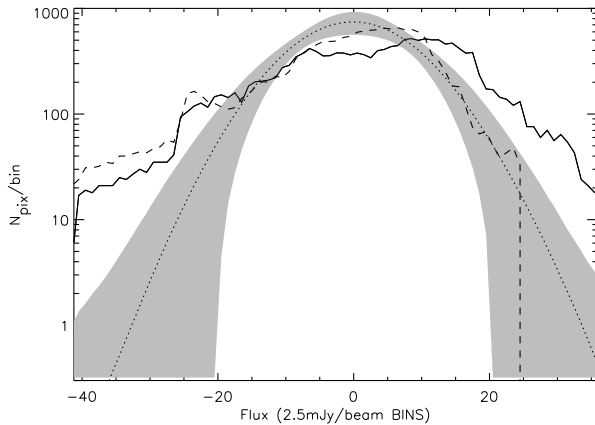


**Figure 4.** Histogram comparing the flux distribution inside the  $1.2^\circ$  FWHM of the primary beam in the 15000 simulations (dotted curve) and in the real data of pointing CrB-H-spot (solid and dashed curves, respectively for the dirty and CLEAN maps). We also show the  $1\sigma$  error bars of the simulations (dashed region).

by the SS in the sources observed in this region (equation (1) of GS05).

We performed a fluctuation analysis similar to Rubiño-Martín & Sunyaev (2003). In Fig. 4 we show a logarithmic plot of the histograms, i.e. the  $P(D)$  functions, of pixel values inside the primary beam  $1.2^\circ$  FWHM from the

15000 simulations (dotted curve) in comparison with the corresponding distribution of the real data (solid curve). For negative fluxes below  $\sim -20 \text{ mJy beam}^{-1}$  the real data shows a clear excess with regards to the simulations, caused by the presence of decrement H. In the positive flux tail a similar excess is found, which stems from the positive spots around the decrement, especially from the one located towards the southeast (see Fig. 1). However, this is an artificial effect, as we explained in detail in GS05. On one hand, the response of an interferometer has zero mean, so the presence of a strong negative feature in the map may enhance the neighbouring positive spots. On the other hand, the convolution of the synthesized beam may give rise to positive features around the strong negative decrement. Note here that we have not applied the deconvolution of the synthesized beam to the simulations, so in Fig. 4 we have represented the flux distribution on the dirty maps. When the flux distribution on the CLEAN map is plotted (dashed line) the excess of the real data in the positive flux tail clearly vanishes, while the excess in the negative flux tail remains.

The percentage of realizations in which the minimum CMB flux value is below that found in the real map is 0.19%. Although a factor of two lower, this value is of the order of that obtained when the equivalent study was applied to the extended configuration data (GS05). We computed in the simulations the standard deviations of all pixels within the primary beam FWHM in order to estimate the confusion level introduced by each component, finding:  $\sigma_{\text{CMB}} = 6.6 \text{ mJy beam}^{-1}$ ,  $\sigma_n = 4.8 \text{ mJy beam}^{-1}$  and  $\sigma_{\text{sour}} = 2.5 \text{ mJy beam}^{-1}$ . Adding these in quadrature we obtain  $\sigma = 8.6 \text{ mJy beam}^{-1}$ , from which we conclude that decrement H is a  $4.8\sigma$  deviation.

We have also computed the power spectrum of pointing CrB-H-spot, following the procedure described in Hobson & Maisinger (2002). The result is shown in Fig. 5, along with that obtained from the last published primordial CMB observations with the VSA (Dickinson et al. 2004) and, for comparison, the theoretical power spectrum that we have used in the simulations. In the first bin, at  $\ell \approx 500$ , the power spectrum of the CrB-H-spot pointing shows a  $4.0\sigma$  deviation from the pure primordial CMB behaviour. This is caused by the presence of the decrement, as this angular scale corresponds to its size, and is similar to the  $2.4\sigma$  deviation at  $\ell \approx 550$  obtained from the extended configuration data (GS05).

These analyses clearly highlight the non-Gaussian nature of this decrement, and show that it is unlikely to be caused by a primordial CMB fluctuation, confirming the results obtained in GS05. Therefore, as the possibility of an unknown galaxy cluster seems implausible (see above), the hypothesis of a large filament pointing towards us is reinforced. The conclusions about the physical shape, density and temperature that this hypothetical structure may have are similar to those put forward in GS05. Essentially, a short filament located inside the CrB-SC and with an electron temperature within the typical WHIM range ( $0.01 - 1 \text{ keV}$ ), can not account itself for the total SZ signal, without any significant X-ray emission. However, we may consider that the total decrement could be a combination of a negative primary anisotropy and an SZ effect. In fact, this decrement is detected in the 214 GHz channel (close to 218 GHz, the null of the thermal SZ effect) of MITO (Battistelli et al.



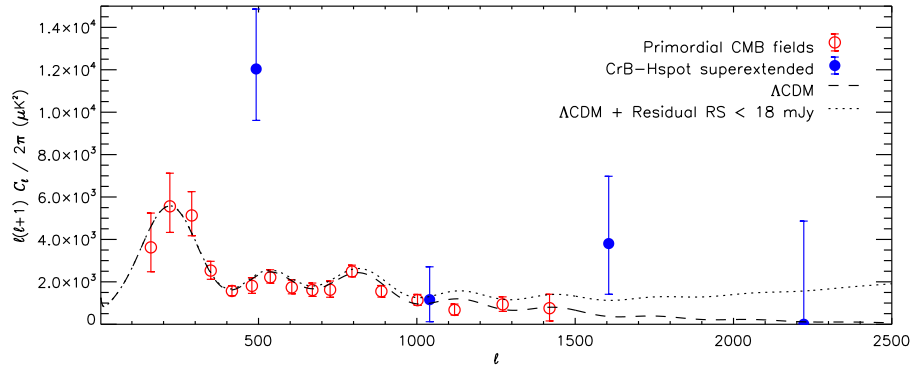


**Figure 5.** Power spectrum computed from the pointing CrB-H-spot (filled circles, blue online), in comparison with that obtained from the VSA primordial fields observations (Dickinson et al. 2004; open circles, red online). We also plot a  $\Lambda$ CDM power spectrum (generated as explained in section 5), with and without the contribution from residual radio sources below 18 mJy. The strong deviation at  $\ell \approx 500$  is due to the presence of decrement H.

2006), indicating that there might be a primordial component. These MITO observations yield that a relative fraction  $f = 0.25$  of the total decrement is produced by a thermal SZ effect. However, up to  $f \approx 0.7$  could be produced by this effect within the typical WHIM temperatures and without a significant X-ray emission. If, for instance, we assume that half ( $f = 0.5$ ) of the decrement is due to the SZ effect from a short filament with electron temperatures  $T_e \sim 0.6 - 0.8$  keV, then baryon overdensities of the order  $\delta\rho_B/\langle\rho_B\rangle \sim 1000 - 1200$  would be needed. These values are in tension with the results of  $N$ -body galaxy formation simulations, which predict that most of the WHIM baryons (70% – 80%) lie in baryon overdensities within the range 5 – 200 (Davé et al. 2001). However, there is still a significant WHIM fraction at  $\delta\rho_B/\langle\rho_B\rangle \sim 1000$  (see Fig. 4 of Davé et al. (2001)), and therefore overdensities of this order are also possible. If we consider a larger filament, then these restrictions are relaxed. We could think of a filament connecting the CrB-SC with the region at  $z \approx 0.11$  where Padilla-Torres et al. 2008 (in prep.) have found a large concentration of infrared galaxies. It would have a length of  $\approx 130$  Mpc, hold a gas mass  $M_{\text{gas}} \approx 10^{15} M_\odot$ , and could produce an SZ decrement as deep as the structure detected in the map ( $f = 1.0$ ) without a detectable X-ray emission. However, according to the simulations, it is difficult to find filaments of this size. This fact, together with the required high elongation along the line of sight, make this structure rather unlikely.

It is worthwhile to examine the WMAP maps in the position of decrement H. In the top panels of Fig. 6 we show the WMAP 5-year temperature maps corresponding to the frequency bands Q, V and W (Hinshaw et al. 2008), centred on the coordinates of CrB-H-spot pointing. The temperature towards the centre of these maps seem to be mostly negative, at a level of  $\sim -150 \mu\text{K}$ . However, it is clear that owing to the coarser angular resolution and lower signal-to-noise of the WMAP data a detailed comparison with our maps is difficult to perform. In order to obtain a more realistic comparison we have convolved these maps with the VSA synthesized beam. To do this we have multiplied the WMAP maps by the VSA primary beam, inverse-Fourier-transformed them to the aperture plane, sampled the visi-

bilities in the  $uv$  points of the CrB-H-spot stack, and finally Fourier-transformed them to the map plane. As a consequence of this, the resulting maps, which are shown in the bottom panels of Fig. 6, contain only the angular scales sampled by the overlapping of WMAP and VSA window functions. In these maps the decrement H appears at a high level of significance, especially in the Q and W frequency bands.

The VSA  $uv$ -tapered map shown in the bottom-left corner of Fig. 1 has a synthesized beam with  $\text{FWHM} \approx 15.3' \times 10.5'$  (in two orthogonal directions). This is comparable to the  $13.2'$  FWHM of the WMAP W-band beam, and indeed both beams subtend the same solid angle. Therefore, a comparison between the temperature values derived from both maps is reliable. The minimum flux in the VSA map is found at position  $\text{RA} = 15^{\text{h}}22^{\text{m}}20.62^{\text{s}}$ ,  $\text{Dec.} = +28^\circ59'06.2''$  (J2000) and corresponds to a brightness temperature (RJ) of  $-197 \pm 35 \mu\text{K}$ . The thermodynamic temperature in the WMAP map on this position is  $-151 \pm 66 \mu\text{K}$ , which, at the frequency of 94 GHz of the W band, is equivalent to a brightness temperature of  $-120 \pm 53 \mu\text{K}$ . Therefore, the VSA and WMAP temperature values agree at a level of  $1.2\sigma_n$ . On the other hand, taking into account that the ratio of the SZ spectrum for the brightness temperature between 33 GHz and 94 GHz is  $1.51^3$ , the WMAP value would correspond to a brightness temperature at 33 GHz of  $-182 \pm 80 \mu\text{K}$ . Therefore, the VSA and WMAP values are compatible within their error bars with an SZ effect.

There are many other mechanisms producing primary or secondary anisotropies which are worth discussing here, although they usually lead to CMB fluctuations either weaker or on smaller angular scales than those produced by the thermal SZ effect.

*Kinetic SZ.* It is well known that in galaxy clusters the kinetic SZ effect is much lower than the thermal com-

<sup>3</sup> This number has been obtained by considering the SZ effect spectrum for the brightness temperature,

$$h(x) = \frac{x^2 e^x}{(e^x - 1)^2} \left[ x \frac{e^x + 1}{e^x - 1} - 4 \right]$$

with  $x = h\nu/(k_B T)$ , between the WMAP ( $\nu = 94$  GHz) and VSA ( $\nu = 33$  GHz) frequencies.



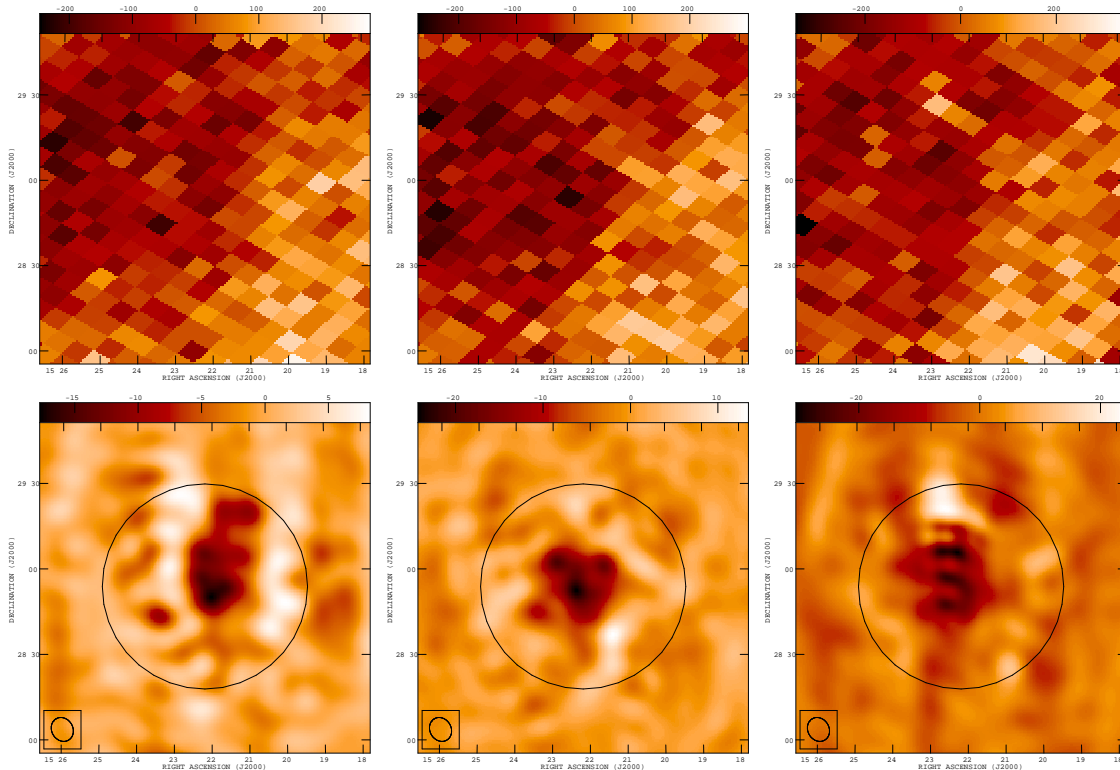


**Figure 6.** WMAP 5-year maps (Hinshaw et al. 2008) in the region of pointing CrB-H-spot. In the top panels the foreground reduced maps of bands Q, V and W (from left to right) are depicted. The maps in the bottom panels have been obtained by multiplying and convolving the top maps with the VSA primary and synthesized beams, respectively. The units of the colour-scale are  $\mu\text{K}$  in the top panels and  $\text{mJy beam}^{-1}$  in the bottom panels.

ponent, typically an order of magnitude smaller. However, at lower electron temperatures, like those of the WHIM, both components become comparable. In a recent work Atrio-Barandela, Mückel & Génova-Santos (2008) argued that the kinetic SZ effect generated in WHIM structures could have an important contribution. They estimate that 1% of all WHIM filaments of size  $\sim 5$  Mpc, aligned with the line-of-sight, produce a combined thermal and kinetic SZ effect that could account for the total flux density observed in decrement H. In particular, a filament of size  $L \approx 5$  Mpc and electron density  $n_e \approx 10^3 \text{ m}^{-3}$  could produce a combined thermal and kinetic SZ signal of  $\approx -200 \mu\text{K}$ . However, a structure like this should produce an X-ray signal detectable in the *ROSAT* data.

*Cosmic texture.* Also recently Cruz et al. (2007) argued that the “cold spot” detected in WMAP data (Vielva et al. 2004) could be caused by a texture, a type of cosmic defect due to symmetry-breaking phase transitions in the early Universe that may produce positive and negative features on the CMB (Turok & Spergel 1990). This spot has an angular size of  $\approx 10^\circ$ , and a minimum thermodynamic temperature of  $\approx -550 \mu\text{K}$  in Q, V and W bands. The predicted number of textures is proportional to  $\theta^{-2}$  ( $\theta$  being its angular size), so many more spots like this are expected in the sky at lower angular scales. Therefore, this phenomenon must be regarded as an alternative explanation for decrement H. Equation (15) of Turok & Spergel (1990) allow us to estimate the number of textures expected in the whole sky of a given angular size. Using that formalism we estimate that

the number of textures of size between 10 and 40 arcmin (the angular scale of decrement H) in the whole area initially surveyed in the CrB-SC ( $24 \text{ deg}^2$ ) is 0.3. In the total area surveyed by the VSA, combining the CrB-SC survey with the primordial fields observations ( $82 \text{ deg}^2$ ; Dickinson et al. 2004), where no features of the size and amplitude of decrement H have been found, the total number expected is 1.2. Therefore, it would be likely to find a structure of this size in the total area observed by the VSA. However, it must be noted that different small-scale processes such as photon diffusion could smear out textures at sub-degree angular scales. Current simulations have not enough angular resolution to study such small angular scales, so it is not clear whether textures of this size could exist.

*Lensing of the CMB.* A massive structure like the CrB-SC could lens the CMB photons, leading to distortions on the mean CMB temperature. However, these distortions are usually small. Even in the richest galaxy clusters, CMB lensing has a characteristic amplitude of a few microkelvins, although its angular size can extend out to a fraction of a degree (Seljak & Zaldarriaga 2000; Holder & Kosowsky 2004). In superclusters like CrB, with much lower densities in the inter-cluster medium, and whose member clusters are not very rich, even lower signals are expected. Therefore, a temperature fluctuation of  $\approx -300 \mu\text{K}$  like decrement H can not be explained in any way by this effect.

*Integrated Sachs-Wolfe and Rees-Sciama effects.* When CMB photons cross time-varying potentials they are blue (in decreasing potentials) or red-shifted (in increasing po-

tentials). This mechanism is known as the Integrated Sachs-Wolfe (ISW) or the Rees-Sciama (RS) effect, when the density fluctuation associated with the time-varying potential is evolving in the linear or non-linear regime, respectively. These effects build up anisotropies in the CMB in the direction of extremely massive structures or voids, typically at large angular scales ( $\gtrsim 5^\circ$ ) and with amplitudes of the order of a few microkelvins (see, e.g., Martínez-González & Sanz 1990; Puchades et al. 2006). With such angular scales and amplitudes this effect is not likely to have a significant contribution to decrement H. However, Dabrowski et al. (1999) studied the physical properties a galaxy cluster may have to produce a combined SZ and RS signal which could account for the CMB decrement detected by Jones et al. (1997) in the direction of the quasar pair PC 1643+4631 A&B without X-ray emission, and found a more significant RS signal. According to their calculations a galaxy cluster at  $z = 1$  with  $T_e \sim 1.3$  keV and enclosing a total mass of  $\sim 10^{16} M_\odot$ , would produce SZ and RS effects respectively of the order  $\sim 500 \mu\text{K}$  and  $\sim 250 \mu\text{K}$  without a significant X-ray emission. But, as we have remarked, a distant cluster is not a likely explanation for decrement H owing to its large angular size.

## 6 CONCLUSIONS

We have carried out observations at 33 GHz with the VSA superextended configuration in the direction of a very deep decrement previously detected by observations with the VSA extended configuration in the CrB-SC (GS05), in a region with no known galaxy clusters and without a clear excess of X-ray emission. Our results clearly confirm the presence of this strong decrement, with flux density of  $-41 \pm 5 \text{ mJy beam}^{-1}$  ( $-258 \pm 29 \mu\text{K}$ ) and coordinates  $\text{RA} = 15^{\text{h}}22^{\text{m}}11.47^{\text{s}}$ ,  $\text{Dec.} = +29^\circ00'06.2''$  (J2000). It has an angular size of about  $30 \times 20 \text{ arcmin}^2$ , being clearly resolved by the superextended configuration synthesized beam ( $\text{FWHM} \approx 7 \text{ arcmin}$ ).

We have confirmed that this deep decrement is detected in the WMAP 5-year maps, but at a much lower level of significance as a consequence of WMAP's lower angular resolution and signal-to-noise. The temperature at the position of the decrement in the W-band map agrees at a level of  $1.2\sigma_n$  with the VSA value, but both temperatures are consistent with a SZ spectrum within their error bars.

A study based on simulations of VSA observations has confirmed its non-Gaussian nature. This study has shown that it is a  $4.8\sigma$  fluctuation, where sigma here includes the confusion noises introduced by the primordial Gaussian CMB, thermal noise and residual radio sources. The probability of this decrement being entirely produced by a combination of these three components is only 0.19%. Therefore an alternative explanation needs to be proposed, and we considered the most likely to be the SZ effect. A galaxy cluster, respectively rich and close enough to produce such a deep and large decrement, would probably have already been detected by existing optical or X-ray surveys. Therefore, this SZ effect could be produced in a less dense and hot structure such as the WHIM. In order to produce such a deep decrement without a significant X-ray emission a filamentary structure with an elongation along the line-of-sight of

about 100 Mpc and a baryon overdensity of 500-800 would be required. These numbers lie close to the top limit of what is expected in these kind of structures, so a filament like this would be rather unlikely. However, if we consider that the total decrement could be a combination of both a primordial CMB fluctuation and an extended SZ effect, then we could have a structure with a size, density and temperature typical of WHIM producing about the half of the minimum flux.

This study reinforces the conclusions addressed in GS05. We are confident that our measurements do show an excess decrement with regard to the primordial CMB. To explain this decrement we require an SZ effect, probably generated in a large-scale WHIM structure. If confirmed, this would have been the first direct detection of an SZ effect from these structures. This would encourage searches for similar structures in other superclusters by other CMB experiments. If they are found, then a significant fraction of the missing baryons in the Local Universe will have been identified.

## REFERENCES

- Atrio-Barandela, F., Mückel, J. P., & Génova-Santos, R. 2008, *ApJ*, 674, L61
- Banday, A. J., Gorski, K. M., Bennett, C. L., Hinshaw, G., Kogut, A., & Smoot, G. F. 1996, *ApJ*, 468, L85
- Barcons, X., Paerels, F. B. S., Carrera, F. J., Ceballos, M. T., & Sako, M. 2005, *MNRAS*, 359, 1549
- Battistelli, E. S., et al. 2006, *ApJ*, 645, 826
- Birkinshaw, M. 1999, *Phys Rep*, 310, 97
- Bolton, R. C., Chandler, C. J., Cotter, G., Pearson, T. J., Pooley, G. G., Readhead, A. C. S., Riley, J. M., & Waldram, E. M. 2006, *MNRAS*, 370, 1556
- Burles, S., Nollett, K. M., & Turner, M. S. 2001, *ApJ*, 552, L1
- Carlstrom, J. E., Holder, G. P., & Reese, E. D. 2002, *ARA&A*, 40, 643
- Cen, R., & Ostriker, J. P. 1999, *ApJ*, 514, 1
- Cen, R., & Ostriker, J. P. 2006, *ApJ*, 650, 560
- Condon, J. J., Cotton, W. D., Greisen, E. W., Yin, Q. F., Perley, R. A., Taylor, G. B., & Broderick, J. J. 1998, *AJ*, 115, 1693
- Cruz, M., Turok, N., Vielva, P., Martínez-González, E., & Hobson, M. 2007, *Science*, 318, 1612
- Dabrowski, Y., Hobson, M. P., Lasenby, A. N., & Doran, C. 1999, *MNRAS*, 302, 757
- Davé, R., et al. 2001, *ApJ*, 552, 473
- Dickinson, C., et al. 2004, *MNRAS*, 353, 732
- Dunkley, J., et al. 2008, *ArXiv e-prints*, 803, arXiv:0803.0586
- Finoguenov, A., Briel, U. G., & Henry, J. P. 2003, *A&A*, 410, 777
- Fosalba, P., Gaztañaga, E., & Castander, F. J. 2003, *ApJ*, 597, L89
- Fukugita, M., Hogan, C. J., & Peebles, P. J. E. 1998, *ApJ*, 503, 518
- Génova-Santos, R., et al. 2005, *MNRAS*, 363, 79
- Grainge, K., et al. 2003, *MNRAS*, 341, L23
- Gregory, P. C., Scott, W. K., Douglas, K., & Condon, J. J. 1996, *ApJS*, 103, 427

- Hernández-Monteagudo, C. & Rubiño-Martín, J. A. 2004, MNRAS, 347, 403
- Hernández-Monteagudo, C., Genova-Santos, R., & Atrio-Barandela, F. 2004, ApJ, 613, L89
- Hernández-Monteagudo, C., Trac, H., Verde, L., & Jimenez, R. 2006, ApJ, 652, L1
- Hill, R. S., et al. 2008, ArXiv e-prints, 803, arXiv:0803.0570
- Hinshaw, G., et al. 2008, ArXiv e-prints, 803, arXiv:0803.0732
- Hobson, M. P., & Maisinger, K. 2002, MNRAS, 334, 569
- Holder, G., & Kosowsky, A. 2004, ApJ, 616, 8
- Jones, M. E., et al. 1997, ApJ, 479, L1
- Lancaster, K., et al. 2005, MNRAS, 359, 16
- Lewis, A., Challinor, A., & Lasenby, A. 2000, ApJ, 538, 473
- Martínez-Gonzalez, E., & Sanz, J. L. 1990, MNRAS, 247, 473
- Mason, B. S., et al. 2003, ApJ, 591, 540
- Mather, J. C., Fixsen, D. J., Shafer, R. A., Mosier, C., & Wilkinson, D. T. 1999, ApJ, 512, 511
- Myers, A. D., Shanks, T., Outram, P. J., Frith, W. J., & Wolfendale, A. W. 2004, MNRAS, 347, L67
- Nicastro, F., et al. 2002, ApJ, 573, 157
- Nicastro, F., et al. 2005, Nature, 433, 495
- Puchades, N., Fullana, M. J., Arnau, J. V., & Sáez, D. 2006, MNRAS, 370, 1849
- Rauch, M., et al. 1997, ApJ, 489, 7
- Rebolo, R., et al. 2004, MNRAS, 353, 747
- Rubiño-Martín, J. A., & Sunyaev, R. A. 2003, MNRAS, 344, 1155
- Scheuer, P. A. G. 1957, Proceedings of the Cambridge Philosophical Society, 53, 764
- Seljak, U., & Zaldarriaga, M. 2000, ApJ, 538, 57
- Scott, P. F., et al. 2003, MNRAS, 341, 1076
- Softan, A. M., Freyberg, M. J., & Hasinger, G. 2002, A&A, 395, 475
- Sunyaev, R. A., & Zeldovich, Y. B. 1972, Comments on Astrophysics and Space Physics, 4, 173
- Turok, N., & Spergel, D. 1990, Phys.Rev.Lett, 64, 2736
- Vielva, P., Martínez-González, E., Barreiro, R. B., Sanz, J. L., & Cayón, L. 2004, ApJ, 609, 22
- Waldram, E. M., Pooley, G. G., Grainge, K. J. B., Jones, M. E., Saunders, R. D. E., Scott, P. F., & Taylor, A. C. 2003, MNRAS, 342, 915
- Watson, R. A., et al. 2003, MNRAS, 341, 1057
- Zappacosta, L., Maiolino, R., Mannucci, F., Gilli, R., & Schuecker, P. 2005, MNRAS, 357, 929

This paper has been typeset from a  $\text{\LaTeX}$  file prepared by the author.